Journal of Materials Science & Technology 213 (2025) 98–108

Contents lists available at ScienceDirect

Journal of Materials Science & Technology

journal homepage: www.elsevier.com/locate/jmst

Research Article

Modeling segregated solutes in plastically deformed alloys using coupled molecular dynamics-Monte Carlo simulations

Hariprasath Ganesan[a,c,1,*], Godehard Sutmann[b,c]

[a] Institute for Advanced Simulation - Materials Data Science and Informatics (IAS-9), Forschungszentrum Jülich, Jülich, Germany
[b] Jülich Supercomputing Centre (JSC), Institute for Advanced Simulation (IAS), Forschungszentrum Jülich, Jülich, Germany
[c] Interdisciplinary Centre for Advanced Materials Simulation (ICAMS), Ruhr-University Bochum, Bochum, Germany

ARTICLE INFO

Article history:
Received 30 April 2024
Revised 18 June 2024
Accepted 18 June 2024
Available online 6 July 2024

Keywords:
Molecular dynamics
Monte Carlo
Virtual atoms
Solute segregation
Cottrell atmosphere
Off-lattice

ABSTRACT

A microscopic understanding of the complex solute-defect interaction is pivotal for optimizing the alloy's macroscopic mechanical properties. Simulating solute segregation in a plastically deformed crystalline system at atomic resolution remains challenging. The objective is to efficiently model and predict a physically informed segregated solute distribution rather than simulating a series of diffusion kinetics. To address this objective, we coupled molecular dynamics (MD) and Monte Carlo (MC) methods using a novel method based on *virtual* atoms technique. We applied our MD-MC coupling approach to model off-lattice carbon (C) solute segregation in nanoindented Fe-C samples containing complex dislocation networks. Our coupling framework yielded the final configuration through efficient parallelization and localized energy computations, showing C Cottrell atmospheres near dislocations. Different initial C concentrations resulted in a consistent trend of C atoms migrating from less crystalline distortion to high crystalline distortion regions. Besides unraveling the strong spatial correlation between local C concentration and defect regions, our results revealed two crucial aspects of solute segregation preferences: (1) defect energetics hierarchy and (2) tensile strain fields near dislocations. The proposed approach is generic and can be applied to other material systems as well.

1. Introduction

Metals, especially alloys, remain critical and widely applied engineering materials. Alloys result from the controlled addition of other chemical elements (*solutes*) to the host system (*solvent*). Consequently, these materials have significant defects resulting from alloying, heat treatments, and processing techniques. Dislocations are linear defects, and their mobility characterizes the plastic deformation behavior. Due to low solubility and interaction with the strain fields, solute atoms segregate near dislocations and other defects, forming a cloud-like distribution called Cottrell atmosphere [1]. The resulting microscopic solute-defect interactions in alloys tend to enhance the material system's macroscopic properties. Thus, a comprehensive understanding of the complex solute-defect interaction is pivotal for optimizing the alloy's target property.

Despite recent advances in characterization techniques [2–6], the complete sequential *in situ* investigation of dislocation nucleation, solute segregation, and the resulting solute-defect interactions remain inaccessible to experiments, owing to the associated time and length scales. Atomistic simulation method like classical molecular dynamics (MD) aids the understanding of such complex solute-defect interactions, still including the interplay between chemical, thermal, and mechanical contributions encountered in the processing conditions [7–13]. MD can faithfully simulate the nanomechanics underlying plastic deformation, i.e., dislocation nucleation, reactions, and mobility within its accessible timescale (ps-μs) and the adequacy of the system's interatomic potential. Solute segregation results from a series of uncorrelated and orchestrated diffusion events spanning several orders of magnitude in time. To this end, simulating solute segregation beyond MD's timescale remains challenging.

MD is often combined with a non-deterministic atomistic method like Monte Carlo (MC) to overcome this limitation and such hybrid approaches simulate rare events like solute diffusion and the resulting segregation [14–23]. At the core of MC, we explore the configuration space through a combination of stochastic

* Corresponding author.
E-mail address: h.ganesan@fz-juelich.de (H. Ganesan).
URL: https://www.fzj.de (H. Ganesan)
[1] Currently at Forschungszentrum Jülich

https://doi.org/10.1016/j.jmst.2024.06.030

trial moves and subsequent evaluation of the acceptance probability of the resulting atomic configuration. For our problem of interest, MC's trial move involves randomly selecting the potential target sites for diffusing solute atoms. Other MC works [19,24–26] follow the on-lattice approach, where the target sites correspond to regular geometric grid points representing the material. However, such strict on-lattice assumptions hold only for an ideal defect-free system. Consequently, detecting target diffusion sites with such an on-lattice assumption becomes invalid and error-prone when the system undergoes severe plastic deformation. MC sampling requires a series of precomputations to identify target sites, even for the most straightforward defect configuration with isolated single dislocations. To this end, previous studies to model solute segregation were severely restricted regarding chemical and defect complexity besides poor computational scalability. Furthermore, the existing approaches [19,24,26] cannot capture potential off-lattice target sites accounting for the dynamic defect environment. Herein, the term 'off-lattice' refers to material representation as an arbitrary collection of points/atoms/particles, unlike the fixed geometric points in space considered for the on-lattice assumption.

Using atomistic simulations, our research question is to model solute segregation in alloys containing arbitrary defects. Herein, a new simulation framework that couples MD and MC was developed using *virtual* atoms to overcome the limitations of timescale and on-lattice sampling. Precisely, the aim is not to simulate the kinetics of several solute diffusion events but to obtain a physically informed segregated configuration, i.e., Cottrell atmosphere (*inhomogeneous distribution of solute atoms*) in the vicinity of crystalline defects. Furthermore, the parallelization of this coupling framework enables a scalable and physically robust approach to simulate complex crystalline defects in the realm of atomistic simulations, thus, a step closer to reality. Also, this framework enables the modeling of solute segregation in complex, generic, and dynamic defect environments. This study applied the MD-MC coupling framework to model C solute segregation in a plastically deformed α-Fe (ferrite) with a body-centered cubic (bcc) crystal structure and ultra-low C concentration.

This article is structured as follows: Section 2 introduces the concept of *virtual* atoms and their behavior along with necessary modifications in MD code base and interatomic potential to ensure physically reasonable and chemically accurate simulations. The last part discusses the realization of MD-MC coupling besides highlighting the dual role of *virtual* atoms. Section 3 validates the uni-directional chemical interaction of *virtual* atoms with the host Fe-C system, followed by demonstrating their ability to detect energetically favorable sites still accounting for local lattice distortion. The final part presents the results of MD nanoindentation to simulate plastic deformation, followed by modeling C solute segregation in a plastically deformed Fe-C system using MD-MC coupling.

2. Materials and methods

2.1. Atomistic modeling - virtual atoms

Segregation refers to inhomogeneously distributed high concentrations of solute atoms near crystalline defects. At the nanoscale, the interaction between segregated solutes and crystalline defects leads to macroscopic phenomena like an increase in yield strength.

Unraveling the atomistic understanding of such interaction poses two requirements:

- Modeling the distribution of segregated solutes,
- Simulating the chemo-mechanics of the segregated solutes with defects (e.g., dislocations, surface, and grain boundaries).

Thermodynamics govern alloys' solid solution type (i.e., substitutional and interstitial), accounting for the host crystal structure and constituent atom sizes. In the substitutional type, solute atoms tend to replace the host atoms at lattice sites. Conversely, solute atoms prefer at or near off-lattice sites for the interstitial type, such as the tetrahedral/octahedral sites or in their vicinity. Herein, we intend to model C atoms (interstitial solutes) segregation in α-Fe (solvent) with a bcc crystalline structure.

In some past works [19,27], modeling solute segregation involved finding the minimum energy site for each solute atom inside the host matrix. Such a modeling approach poses two critical limitations:

- The problem becomes intractable with an increasing simulation system size or a high solute concentration;
- It is extremely challenging to detect a probable solute atom's minimum energy site that still accounts for lattice distortion from crystalline defects in the host structure.

To this end, modeling segregated solutes in the plastically deformed metallic material (i.e., off-lattice) at atomic resolution remains challenging.

We overcome this challenge by introducing a novel concept of *virtual* atoms in the host system (i.e., Fe-C). These *virtual* atoms are fictitious, pseudo atoms exerting uni-directional chemical interaction with the surrounding host system atoms (refer Fig. 1(b)). In principle, *virtual* atoms aim to find energetically favorable off-lattice sites (i.e., representing material as an arbitrary collection of points/atoms/particles) through efficient unbiased sampling, still accounting for crystal lattice distortions from defects. Note that for *virtual* atoms, we assumed the same atomic size and mass as that of solute atoms.

Experiments and first-principle calculations [14,28] predict that C atoms prefer octahedral sites in α-Fe, which is a valid assumption in the defect-free host system. However, this assumption gets invalidated when the host crystalline system undergoes lattice distortion due to defects and their resulting strain field. Consequently, identifying potential occupation sites for solute atoms becomes cumbersome in such scenarios, particularly with some finite solute concentrations. As a starting point, we introduced *virtual* atoms at all octahedral sites in host bcc α-Fe (refer Fig. 1(a)). The so-called *virtual* atoms exert a uni-directional chemical interaction with the surrounding host system containing *real* atoms, i.e., Fe and C. This means that the *virtual* atoms experience the forces from surrounding *real* atoms but not vice-versa (refer Fig. 1(b)). Eventually, the existence/inclusion of *virtual* atoms does not affect the atomic evolution of the host *real* system (i.e., Fe and C atoms) to any degree. Therefore, *virtual* atoms are self-consistently following the strain field in a material, thus enabling the possibility to detect sites close to the minimum energy position for a solute atom.

2.2. Modifications in MD code & extending interatomic potential

The objective of the *virtual* atoms is to find energetically favorable sites in the host atomic neighborhood considering local lattice distortion and strain field exerted by crystal defects. *Virtual* atoms address this objective by adapting self-consistently their positions, still obeying the constraint of uni-directional chemical interaction with the surrounding *real* atoms.

At this point, implementing the concept of *virtual* atoms within the atomistic simulation framework requires two key aspects:

- Physics: Modifications in MD code base to enable the functionality of *virtual* atoms as intended
- Chemistry: Extension of binary interatomic potential (Fe-C) to include *virtual* atoms for defining interatomic interactions, i.e., a *quasi* ternary potential (Fe-C-V). Here, V refers to *virtual*.

In this work, atomistic MD simulations were performed using the classical MD package, IMD [29], which has been extended to

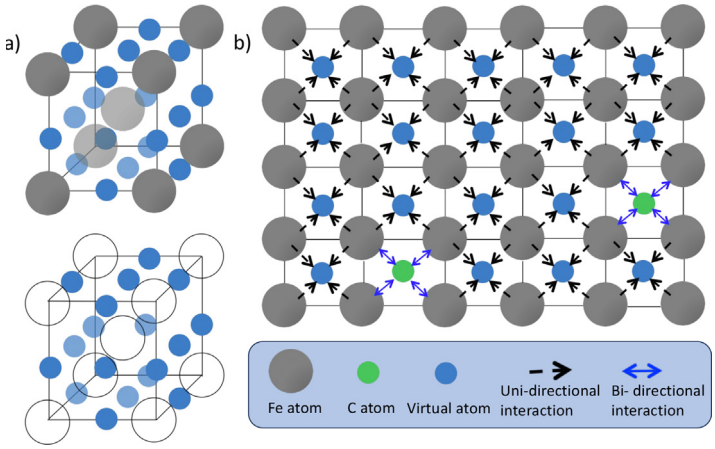

Fig. 1. Introduction of virtual atoms in the host system (a) Top: A body-centered cubic unit cell with Fe atoms (*grey*) at lattice sites and virtual atoms (*blue*) at octahedral sites, Bottom: Fe atoms are hidden for clarity (b) Schematic illustration of special uni-directional interaction of virtual atoms (*blue*) with the surrounding Fe atoms (*grey*) vs. bi-directional interaction a carbon atom (*green*) with surrounding atoms. Here, Fe and C atoms are considered as *real*, whereas blue atoms are *virtual*.

Table 1
Different energy contribution based on atom element type.

atom i	atom j	interaction
real	*real*	atom i and atom j exchange energy
real	*virtual*	atom i exert energy on atom j
virtual	*real*	atom i get energy from atom j
virtual	*virtual*	atom i and atom j exchange energy

handle the functionality of *virtual* atoms. The first core modification is associated with the force computation, as shown in Eq. (1), where a *real* atom exerts some resulting interatomic force on a *virtual* atom as per the gradient of the potential ($\boldsymbol{f}_{real\rightarrow virt} = -\nabla U$), whereas a *virtual* atom exerts no force on a real atom ($\boldsymbol{f}_{virt\rightarrow real} = 0$), as per the constraint of uni-directional interaction. Therefore, force computations are implemented with the following conditions.

$$\boldsymbol{f}_{\mathrm{real}\rightarrow\mathrm{virt}} \neq \boldsymbol{f}_{\mathrm{virt}\rightarrow\mathrm{real}} \tag{1}$$

The second core modification is related to energy computation. Herein, the interactions between Fe-Fe and Fe-C atoms are computed based on the Embedded Atom Method (EAM) [30], which is often used as a classical approximation for metals and alloys. The total potential energy (U_{Total}) of the many-particle (N atoms) system is then computed as

$$U_{\mathrm{Total}} = \sum_{i=1}^{N}\left[\frac{1}{2}\sum_{j\neq i}\phi_{ij}(r_{ij}) + F_i\left(\sum_{j\neq i}\rho_j(r_{ij})\right)\right] \tag{2}$$

where r_{ij} and ϕ_{ij} refer to the interatomic distance and pair interaction energy between the ith and jth atom. N denotes the total number of *real* atoms (i.e., Fe and C) in the system and F_i indicates the embedding energy of the ith atom due to the cumulated host electron density $\sum_{j\neq i}\rho_j(r_{ij})$ provided by the surrounding atoms. The pair interaction energy and electron density are summed over the neighboring j atoms defined by the cutoff radius. To this end, special modifications (refer Table 1) were included to eliminate the energy contributions of *virtual* atoms while computing the localized atomic energy of a *real* atom and the total energy of the system. Note that per definition, *virtual* atoms are non-physical and fictitious, thus contributing no energy to the *real* host system (i.e., Fe and C). For spatial and temporal averaging of *real* systems quantities during the simulations, *virtual* atoms' existence and contributions are not included. Similarly, the contributions from the atomic vibrations of *virtual* atoms were discarded from the kinetic energy of the *real* system.

Another crucial aspect is defining the chemistry of *virtual* atoms. Within the atomistic simulation framework, *virtual* atoms were assigned a distinct chemical type. Herein, we considered EAM [31] potential for the host (*real*) Fe-C system, containing pair interaction (ϕ_{FeFe}, ϕ_{FeC}, ϕ_{CC}), electron density (ρ_{Fe}, ρ_{C}) and embedding function (F_{Fe}, F_{C}). We extended the Fe-C potential with additional pair interaction (ϕ_{FeV}, ϕ_{CV}, ϕ_{VV}), electron density (ρ_{V}), and embedding function (F_{V}) contributions to realize the Fe-C-V potential, thus, enabling the chemical interaction between the *real* and *virtual* atoms. Recall that both *virtual* and solute (i.e., C) atoms possess the same atomic size and mass. Furthermore, *virtual* atoms were expected to chemically behave like C atoms, however, without influencing the surrounding *real* atoms (owing to uni-directional interaction). Therefore, we extended the pair interaction ϕ_{FeV} from ϕ_{FeC}, defined by Ruda et al. [32] to mimic a C-like behavior.

Introducing a C atom at any octahedral (O) site creates short-range lattice distortion in the atomic neighborhood [33] due to bi-directional interaction. However, a *virtual* atom at any O site in a defect-free α-Fe tends to remain at the same site (i.e., $a/2 = 1.4$ Å) due to the force-symmetry from the nearest neighbor atoms. Contrarily, in case of some local lattice distortion from solute local composition or crystalline defects, a *virtual* atom experiences some force asymmetry. Consequently, the *virtual* atom is displaced from its initial position to find the new energetically favorable site. The aforementioned extensions included three components of EAM (refer Eq. (2)), i.e., pair interaction (ϕ), electron density (ρ), and embedding energy (F).

As per Ruda et al. [32], pair interaction ϕ_{CC} has a pure repulsion below 1.9 Å, limiting two C atoms staying closer below this distance. We assumed identical pair interaction part for 'ϕ_{CC}' and 'ϕ_{CV}', thus, defining comparable chemistry between *real* C and *virtual* atoms. Accordingly, a strong repulsion was defined between *virtual* atoms ('ϕ_{VV}') part below 1.4 Å (i.e., $a/2$) and without any attraction part. Such a strong repulsion component (i.e., linear part (< 0.5 Å) and asymptotic part (0.5–1.4 Å)) was necessary to avoid any unphysical overlapping of two *virtual* atoms.

Unlike the pair interaction, which dictates the chemistry between two individual atoms at any instance, the electron density part refers to the contribution of a group of surrounding 'j' atoms on a target atom 'i'. Herein, no chemical contributions of *virtual* atoms (i.e., $\rho_{\mathrm{VFe}} = 0$, $\rho_{\mathrm{VC}} = 0$) were assumed on the real atoms Fe

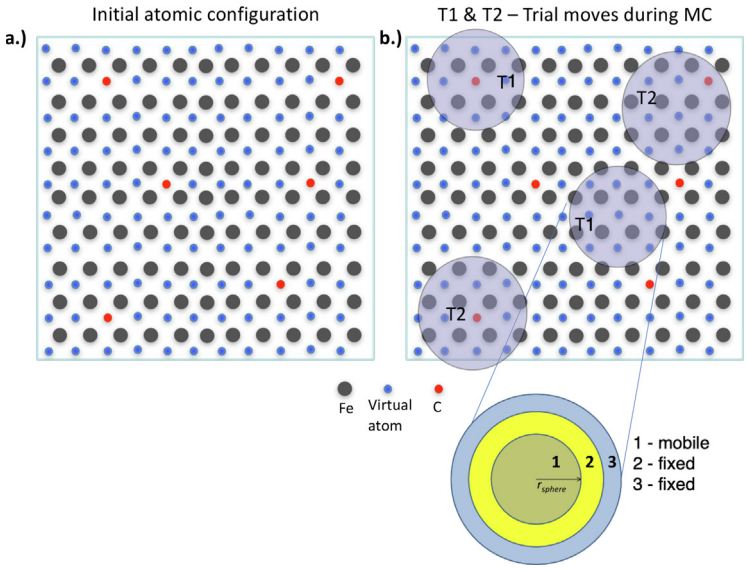

Fig. 2. (a) Initial representative atomic configuration of the defect-free host system composed of *real* atoms (i.e., Fe, C) and *virtual* atoms at all octahedral sites. (b) Illustration of a *swap* type MC trial move steps (e.g., T1, T2) associated with localized energy computation of reference central atoms.

and C. In contrast, the embedding energy contributions by *real* atoms on the *virtual* atoms were considered. Furthermore, the electron density contributions (ρ_V) of *virtual* atoms were included only for other *virtual* atoms as they should not chemically influence real atoms (Fe, C) in the system. To this end, the embedding function F_V and electron density ρ_V were adapted from F_C and ρ_C such that carbon and *virtual* atoms have similar many-body contributions.

2.3. MD-MC coupling: duality of virtual atoms

Investigating the interaction of segregated solutes with crystalline defects at the atomic scale remains challenging. A critical bottleneck is a lack of physically sound, scalable, and unbiased modeling of solute segregation in a host crystalline environment containing arbitrary defects. MD is readily amenable to large-scale atomistic simulation of materials with defects. However, the physically motivated choice of MD timestep (i.e., 1 fs for metals & alloys) to capture fast events like atomic vibrations poses severe spatiotemporal restrictions on physical phenomena that could be studied. Although some parallel computation approaches (e.g., domain decomposition [34]) could lift the length-scale limitation, overcoming the time-scale limitation even partially remains strenuous despite applying some accelerated approaches [35,36]. To this end, MD can reasonably capture phenomena in the ps-μs range using high-performance computing architectures and state-of-the-art GPUs [37]. However, segregation due to several independent and concerted diffusion events span the time scale of seconds to hours, thus, certainly beyond the scope of classical MD. On the other hand, hybrid approaches combining deterministic MD and stochastic MC techniques open some possibilities. Precisely, we are not interested in the kinetics of several solute diffusion events but in the *nearly* final segregated configuration, where it is assumed that configuration space is fully accessible, i.e., inhomogeneous distribution of solute atoms in the vicinity of crystalline defects. However, such time-dependent solid-state phase transitions could also be effectively captured by deploying kinetic MC (requiring some event catalogs) or with some kinetic models like nucleation index-incorporated Johnson-ehl-vrami-olmogorov (NI-JMAK) [38]. Luo et al. [39] and Li et al. [40,41] provided a comprehensive review of such kinetic models. To this end, we developed a consistent atomistic framework coupling classical MD and *Metropolis* MC approach.

The novelty of our MD-MC coupling approach is attributed to the so-called *virtual* atoms, linking these two distinct simulation protocols to realize solute-segregated configurations in atomic systems with complex defect environments. Herein, *virtual* atoms play a dual role within our MD-MC coupling framework. In the scope of MD, *virtual* atoms adapt their positions, sensing any local lattice distortion in the atomic neighborhood due to solute atoms or defects and their combinations. Note such displacements to new positions were possible as a result of uni-directional interaction (refer Section 2.1) with the neighborhood *real* atoms (Fe and C) in the host system. In the scope of MC, those adapted *virtual* atoms positions act as potential sampling sites for evaluating the probability of target solute atoms' occupation.

In this work, we applied a three-fold strategy to realize the *nearly* final segregated configuration of solute C atoms in Fe-C alloys containing arbitrary defects: (1) plastic deformation of the Fe-C alloy model (*with homogeneously distributed C atoms*) using nanoindentation; (2) global energy minimization of the plastically deformed model; (3) applying the MD-MC coupling scheme to stochastically redistribute C atoms in accordance with an acceptance criterion [42,43] to find more energetically favorable sites, eventually obtaining segregated C distribution especially near defect regions. Herein, in our coupling scheme, we combined MD and MC with distinct objectives besides the seamless exchange of information. Furthermore, two levels of MD are being used, namely *global* MD and *local* MD.

***Global* MD**: As a first step, we realized a defect-free α-Fe (bcc) single crystal containing *virtual* atoms at all octahedral sites (refer Section 2.1). After relaxing the initial system, we alloyed the host system with some finite C concentrations (*homogeneously distributed*) by randomly swapping some *virtual* atoms into real C atoms (refer Fig. 2(a)). After subsequent energy relaxation/minimization of the *ternary* system (i.e., Fe, C, V), we performed nanoindentation to introduce some plastic (*irreversible*) deformation in the sample.

***Local* MD**: In the scope of our coupling approach, the term 'local' refers to the energy computations of the spherical atomic regions constructed around the randomly chosen particles/atoms (i.e., a real C atom and a *virtual* atom), during each MC trial move,

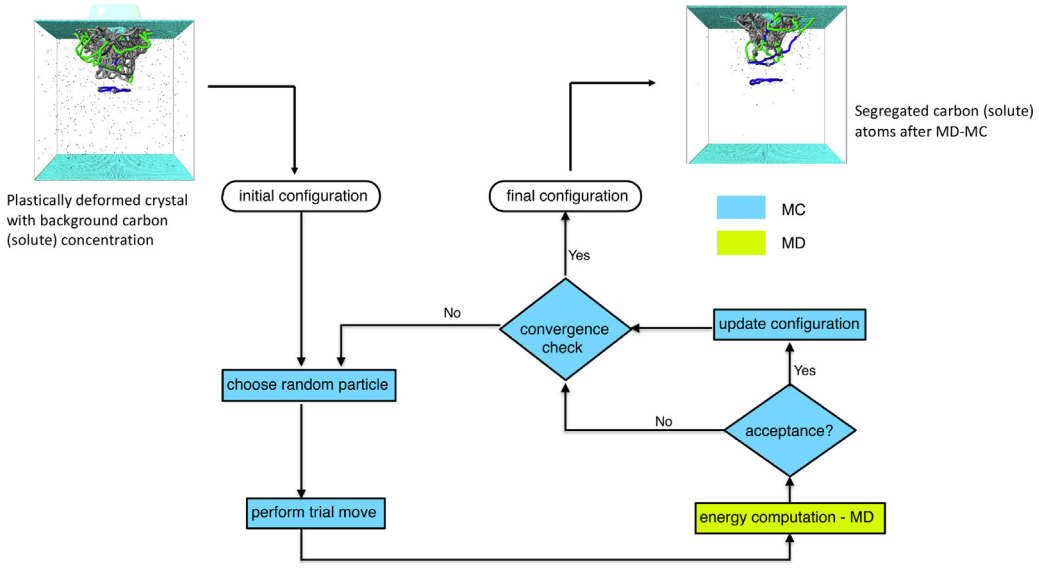

Fig. 3. MD-MC coupling workflow. The *initial* configuration refers to a plastically deformed single crystal containing a complex dislocation network and homogeneously distributed C atoms. Herein, *real* Fe and *virtual* atoms are hidden for clarity. The *final* configuration shows segregated C atoms after n target MC steps (iterations).

as shown in Fig. 2. Specifically, the notion 'local' indicates the finite cut-off radius r_{sphere} around the chosen atom, considered for energy computation (refer Fig. 2). Our assumption of such localized energy computations was physically motivated by the nearsightedness of the lattice perturbation introduced by the insertion or deletion of a C atom. By systematically investigating our Fe-C system with different defect scenarios (e.g., isolated C, C clusters, point defects, dislocations) and solute concentration [44], we assigned the optimal $r_{\text{sphere}} = 2$ nm for all the local MD simulations in this work.

Most importantly, such localized energy computation offers the following advantages: (1) enable parallel execution of trial moves owing to the spatially independent concurrent spherical regions (e.g., refer T1 & T2 in Fig. 2), (2) reduce computational workload as such localized spherical regions contain around 10^3 atoms against the global atomic configurations with $10^6 - 10^8$ atoms, (3) offer the scope for scalability as such energy computations need to be performed for 2×10^6 trial moves, thus, saving significant computation time and resources.

MC Simulations: Such a plastically deformed host atomic system containing *real* (Fe and C) and *virtual* atoms serves as an input for the MC counterpart. Herein, the core MC module consisted of five steps: 1) random particle selection, 2) trial move execution, 3) energy computation using *local* MD, 4) evaluating acceptance criterion, and 5) updating configuration.

During step 1, we randomly selected two particles/atoms (one *real* C atom and one *virtual* atom). Recall that both C and *virtual* atoms possess the same atomic size and mass but different chemical types and interactions (i.e., C atoms with bi-directional vs. *virtual* atoms with uni-directional, refer Section 2.1). Then, in step 2, we performed a trial move (refer Fig. 2) by swapping the positions of selected C and *virtual* atoms (in principle, *stochastically* mimicking the spatiotemporal diffusion event of a C (solute) atom). In subsequent step 3, we evaluated the energy of the atomic neighborhood of the selected atoms after the trial move, i.e., swap. Herein, we introduced the novelty of performing localized energy minimization using *local* MD [42,45]. The atomic neighborhood refers to the spherical spatial region falling within r_{sphere}, as shown in Fig. 2(b). Then, we evaluated the acceptance criterion [43,44] by comparing the atomic energies of the spherical regions *before* and *after* each trial move. Herein, we considered the (modified) Metropolis acceptance criterion (at $T = 0$ K), with an acceptance probability of $P_{\text{acc}} = 1$ (if net energy decreases) and 0 (otherwise). As a last step, we updated the atomic configurations if the acceptance criterion evaluation turned true, i.e., storing the new positions of swapped atoms during the trial move. By definition, the existence of virtual atoms should not influence the energy of the *real* atoms at both the global and local scales. We justified the global one in Section 3.1, where *virtual* atoms were not influencing the real atoms' energetics. In a similar fashion, we also performed some benchmarking for local energy computation, yielding identical results.

Then, we continued with the next MC step, executing trial move T2, and iterated through these five steps until the convergence criterion was satisfied. Eventually, the final atomic configuration, which consisted of redistributed C atoms (solutes), corresponded to segregated solutes (Cottrell atmosphere) near the defect regions.

In this work, we demonstrated the concept of *virtual atoms* with an emphasis on the coupling approach (refer Fig. 3) rather than the complexity of the solute segregation scenario. However, in principle, our approach could be extended to simulate solute segregation in poly-nanocrystalline models constructed by using Voronoi tessellation, where the grain regions represent the crystalline lattice configuration (e.g., Fe-C-V). Note that initial *virtual atoms* could be either at octahedral sites or some randomly rattled positions.

Parallelization of MD-MC coupling: Interestingly, during MC step 3, if these localized atomic regions do not overlap in space (refer to trial moves T1 & T2 in Fig. 2), the energy computations can be done independently from each other, which allows for spatial parallelization of the relaxation process of inserted atoms. Obviously, there might exist scenarios where spherical regions from different trial moves could spatially overlap, thus making the parallel execution of trial moves challenging. To this end, we tackled such changes by developing a robust, computationally efficient, resource-aware, yet physically conforming parallelization scheme for our MD-MC coupling approach. More detailed information on methodological and performance aspects of our parallelization scheme shall be referred from our previous works [43,44,46,47]. Furthermore, we used an in-house visualization tool to visualize the atomic configurations and extract dislocations [48].

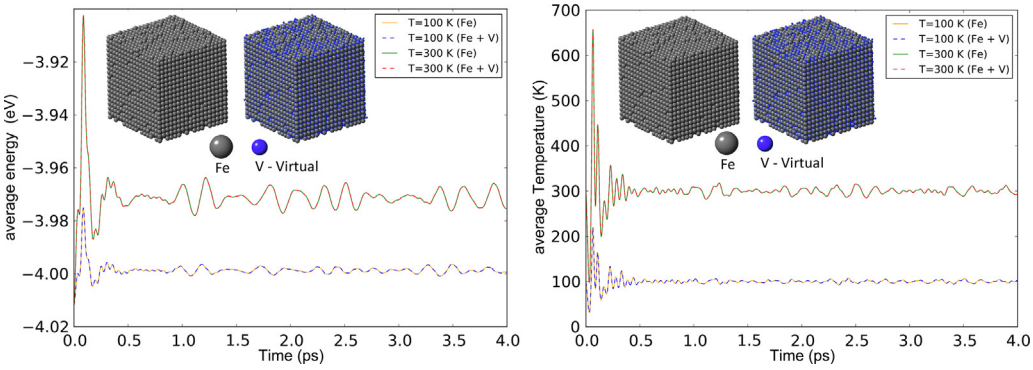

Fig. 4. Comparison of thermodynamic evolution of two topologically identical but chemically different systems (i.e., insets showing System 1 - *real* Fe atoms, System 2 - *real* Fe + *virtual* V atoms). (Left): Temporal evolution of global energy and (Right): Temporal evolution of global temperature for the two systems.

3. Results & discussion

This section encompasses results and in-depth discussions of two aspects:

- Validation of physically reasonable and chemically accurate working of *virtual* atoms
- Realization of C solute segregated configuration using our MD-MC coupling framework in a nanoindented sample (i.e., plastically deformed).

3.1. Validation of virtual atoms interaction with real atoms

As extensively discussed in the Section 2.1, we introduced the concept of *virtual* atoms within our atomistic MD-MC coupling framework. These *virtual* atoms were conceptualized to exhibit uni-directional chemical interactions with the surrounding *real* atoms (e.g., Fe and C) in the *host* crystalline system. In other words, the *host* system should not chemically experience the existence of *virtual* atoms; thus, the global thermodynamic observables of the *real* atomic system during MD simulations must remain unperturbed. To verify this conceptual claim, we performed comparative MD simulations of two topologically identical atomistic systems with the same dimensions (5 nm^3) and underlying crystal structure (bcc). However, system-1 contained only *real* Fe atoms, whereas system-2 contained both *real* Fe atoms and *Virtual* atoms at all the octahedral sites (refer Section 2.1). Furthermore, we evolved these two systems at different temperatures (T = 100, 300 K) under an NVT ensemble with fully periodic boundary conditions.

Fig. 4 compares the evolution of global thermodynamic quantities of these two systems, i.e., system 1 with N_{Fe}- 11664 (*real* Fe atoms), system 2 with N_{Fe}- 11664 *real* Fe atoms and N_V- 34992 (*virtual* atoms). Note that in system-2, we had a *real*/*virtual* atoms ratio of 1:3, indicating three times more octahedral sites than lattice sites. Both systems exhibited identical potential energy and temperature (*both quantities were globally averaged*).

It is worth mentioning that we compared these simulation results generated using two different versions of the IMD code base [29], i.e., the original version (without *virtual* atoms) and the extended version (with *virtual* atoms) to validate the quantitative accuracy including the algorithmic correctness and expected chemical implications. To this end, both the systems were in perfect agreement at both simulated target temperatures of 100 and 300 K (refer Fig. 4), validating the intended uni-directional interaction of *virtual* atoms. Herein, for the final configuration, the *virtual* atoms did not exhibit significant displacements (w.r.t initial octahedral positions) except for thermal oscillations, as the host Fe system was defect-free. In short, the existence of *virtual* atoms did not influence the trajectory of the *real* system, as indicated by the potential energy and temperature evolution of the two systems during MD simulations. Furthermore, these simulation results validate the physical correctness of extensions w.r.t *virtual* atoms made within some of the core MD [29] routines (refer Section 2.2).

3.2. Detecting local lattice distortion and rearrangement behavior of virtual atoms

The prime objective of the *virtual* atoms is to detect energetically favorable sites accounting for local lattice distortion originating due to several sources, including strain fields resulting from crystalline defects, chemical interaction with the constituent species, or externally applied force fields. To demonstrate this objective of the *virtual* atoms, we performed a nanoindentation simulation (spherical indenter, r_{indenter} = 8 nm). The initial atomic configuration represented the defect-free α-Fe bcc system containing *real* Fe atoms and *virtual* atoms at all the octahedral sites (refer Section 2.1). Fig. 5 shows the sliced views of atomic configurations during simulated nanoindentation using *global* MD. Also, to improve visualization, a special focus has been emphasized on the spatial region beneath the indentation contact point (refer to the bottom row in Fig. 5). Herein, the sliced views of MD simulation snapshots include only *virtual* atoms (*blue*) for clarity.

At the start of nanoindentation simulation (refer Fig. 5), when the spherical indenter came in contact with the surface (at t = 20 ps), a vast majority of *virtual* atoms remain undisturbed except a special zone beneath the indenter showing some *virtual* atoms rearrangements in positions. This early observation sounds physically reasonable as the displacement/strain field introduced by the indenter was locally confined in space. Therefore, only the *virtual* atoms in the vicinity showed some recognizable displacements. As the indenter penetrated further into the material sample during the loading phase (at t = 140 ps), the externally induced strain field propagated deeper into the material. At that point, we observed some considerable lattice distortion; thus, relatively more *virtual* atoms undergo displacements from their initial octahedral sites. Such rearrangement behavior demonstrates *virtual* atoms' ability to find energetically favorable sites considering instantaneous lattice distortions in the atomic neighborhood. Note that still, *virtual* atoms located far from the indentation zone (i.e., lower half of the system) remained unperturbed. Unloading the indenter (at t = 340 ps) recovered all the elastic strain, thus leaving only the plastic strain in the system characterized by the existing dislocation networks and some lattice distortions (e.g., vacancies, voids), near which we observed some localized redistribution of *virtual* atoms due to force asymmetry compared to the defect free neighborhood (refer Fig. 5). Note that the sliced view contains only part of the dislocation components. Interestingly, again, most of

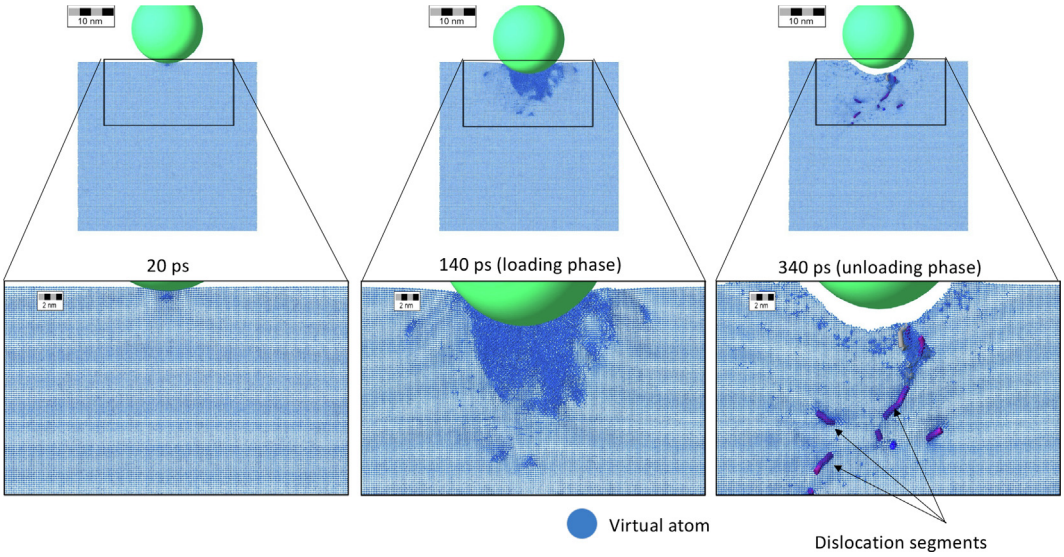

Fig. 5. Sliced views of atomic configurations (*snapshots*) during simulated nanoindentation test, demonstrating *virtual* atom's ability to find new energetically favorable sites considering lattice distortion in the atomic neighborhood. For clarity, only *virtual* atoms (blue) are shown.

the *virtual* atoms rearranged back to their original sites as most of the elastic displacement field was removed from the system. However, the *virtual* atoms captured the traces of plasticity and rearranged in the vicinity of the surface crater, dislocation segments, vacancies, and voids.

These results demonstrate the physical robustness of our *virtual* atoms in sensing the dynamic lattice distortion due to strain fields in the system, which is a salient feature, and their ability to find energetically favorable off-lattice sites governed by uni-directional interaction and extended Fe-C-V potential. Similarly, in our previous works [42,44], we have also demonstrated the robustness of *virtual* atoms in another dynamic defect environment (e.g., the annihilation of defects).

3.3. Nanoindentation and simulating C segregation in plastically deformed crystal using MD-MC coupling:

The overarching goal of our atomistic MD-MC coupling framework using the novel *virtual* atoms is to model segregated solutes in crystalline configurations containing arbitrary defects. Consequently, the effects of the interaction of segregated solutes and crystalline defects on the mechanical deformation behavior of alloy systems could be further investigated.

It is worth emphasizing that the phenomena of plastic deformation (*defect nucleation*) and carbon segregation evolve at different time scales separated by orders of magnitude. Recall that the objective here is not to simulate the kinetics of carbon diffusion events but to realize the *nearly* final atomic configuration containing segregated carbon atoms. Thus, the energy-relaxed atomic configuration containing arbitrary defects (simulated with *Global* MD) will be given as the input for modeling solute segregation (MD-MC coupling). Note that there are significant thermodynamic factors (e.g., free energy minimization, elastic strain energy minimization, chemical bonding, and solute-solute interactions) and kinetic factors (e.g., deformation-induced defects generation (*like vacancies, dislocations, and planar defects*), defect mobility, non-equilibrium segregation, and enhanced diffusion) contributing to the solute segregation in plastically deformed alloys. This work focused extensively on the former factor while indirectly encompassing the latter one.

To this end, we realized solutes segregated configuration in plastically deformed samples in two stages:

1) Plastic deformation using Global MD: In stage 1, using *Global* MD (refer Section 2.3 for details), we simulated nanoindentation to deform the sample plastically, thus introducing some arbitrary defects into the initial defect-free α-Fe system with *real* Fe and *virtual* atoms (at all the octahedral sites). Herein, the simulation domain had a lateral length, $l = 30$ nm, with the crystallographic orientations X [1 0 0], Y [0 1 0], and Z [0 0 1]. We introduced a background C concentration (0.005 wt.%) by swapping some randomly selected *virtual* into *real* C atoms. The initial configuration contained 2.23×10^6 Fe atoms, 6.7106×10^6 *virtual* atoms, and 2×10^3 C atoms. Then, we performed energy minimization to accommodate the local lattice strain caused by homogeneous C distribution. We simulated nanoindentation (spherical indenter, $r_{\text{indenter}} = 6$ nm) on the energetically minimized initial configuration, introducing plastic deformation into the defect-free single crystal. Herein, the Fe-C EAM potential from Veiga et al. [31] was applied for interatomic interactions along with the extended Fe-C-V potential (refer Section 2.1). Along the Z [0 0 1] direction, we assumed free boundary conditions on the top surface and fixed boundary conditions at the bottom, corresponding to the last few atomic layers with a thickness of 1 nm. The spherical indenter was loaded on the material surface along the Z direction at a velocity of 20 m/s for a total duration of 220 ps.

The top row in Fig. 6 shows the dislocation nucleation and production using *global* MD. An avalanche of dislocation segments was created and multiplied as a follow-up stage to sustain the plastic deformation. For visual clarity (refer Fig. 6), the nanoindented samples show only C atoms and introduced dislocations. After unloading, the elastic strain was recovered, thus leaving a plastically deformed intermediate configuration with dislocation networks. Note that *virtual* atoms in the vicinity of dislocations and surface crater (*underneath the indenter*) underwent considerable displacements to detect energetically favorable sites, as extensively discussed in the previous Section 3.2. Herein, the dislocation skeletonizer algorithm introduced by Begau et al. [48] was used to extract the dislocation networks in the deformed sample.

2) Modeling solutes segregation using MD-MC coupling with local MD:

In stage 2, the plastically deformed output configuration from the *global* MD simulation was energetically relaxed and assumed to be the initial configuration for the coupled MD-MC simulations (refer to Fig. 3). Then, we iterated through five steps

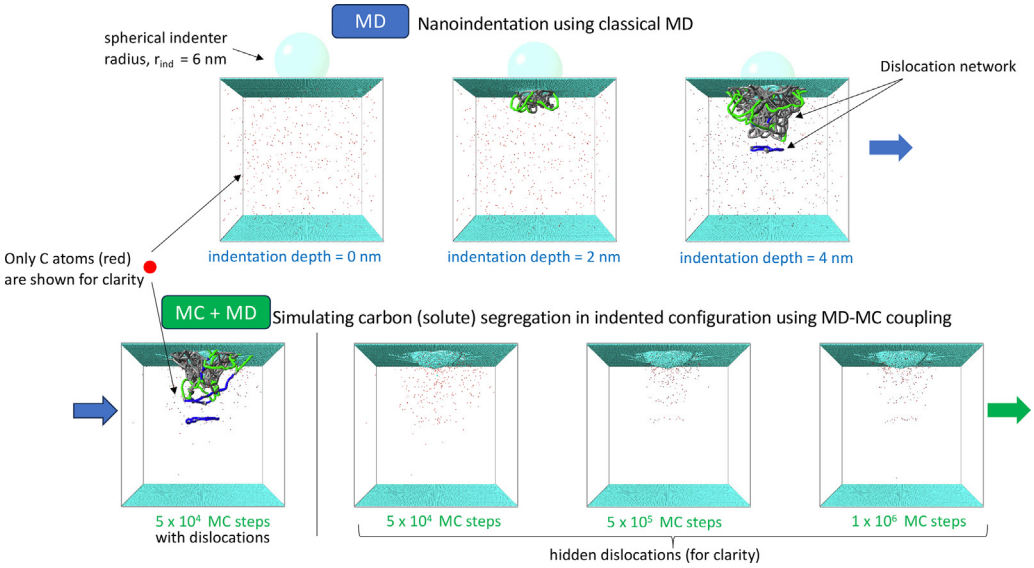

Fig. 6. Top row: *Global* MD simulated nanoindentation snapshots of atomic configurations with the initial defect-free α-Fe single crystal containing 0.005 wt.% C (*homogeneously distributed red atoms*). Bottom row: MD-MC coupling simulated sequence of atomic configurations showing segregated C atoms towards dislocations and surface after different MC steps.

(refer Section 2.3) in the MC core routine, namely: 1.) random particle selection, 2.) trial move execution, 3.) energy computation using ***local*** MD, 4.) evaluating acceptance criterion [43,44], and 5.) updating the configuration. During each MC step, we executed a trial move by randomly choosing one *real* C atom and one V atom with a uniform sampling probability of $1/N_C$ and $1/N_V$ and swapping their positions. Then, we evaluated the energies of the resulting atomic configurations confined in the spherical regions (refer Fig. 2) using local MD. Fig. 6 (bottom row) shows the segregated C atoms after different MC steps (i.e., 5×10^4 MC steps, 5×10^5 MC steps, 1×10^6 MC steps).

Recall that *virtual* atoms assumed a dual role. In the scope of MD, *virtual* atoms detected energetically favorable sites by undergoing displacements; accounting for local lattice distortion (refer Section 3.2), whereas within MC, these *virtual* atoms act as potential sampling sites for executing the swap type trial move. In particular, such rearranged *virtual* atoms near defects bear a high probability of acceptance as they were more energetically preferred. With increasing MC steps and more successful trial moves, we observed more C atoms (*red*) relocated to such new energetically favorable sites. Compared to the initial configuration (from *Global* MD) with homogeneously distributed C atoms, the simulated final configuration using MD-MC refers to a segregated profile (i.e., Cottrell atmosphere) exhibiting non-homogeneous high C concentration near dislocations and the surface.

Through non-local swap type trial moves, we ensured uniform and unbiased sampling. Starting with the initial homogeneous C distribution, the acceptance probability was higher for long-range trial moves. During early MC steps, C atoms distributed in the lower half of the crystal showed a tendency to segregate towards the new energetically favorable sites in the upper half of the crystal with dislocations and surface defects. The resulting solute segregated profile appeared qualitatively correct after 1×10^6 MC steps. However, the physical correctness of the obtained profile needs to be validated considering various aspects. Most of the accepted trial moves were energetically favorable from a thermodynamic standpoint. In other words, the potential energy of the initial configuration (*homogeneous C distribution*) got continually minimized as more C atoms segregated towards or near the dislocation regions. We have earlier reported [42–44] that the solute-segregated profiles (i.e., C Cottrell atmosphere) in the Fe-C system with isolated, perfect dislocations (e.g., screw, edge) using our MD-MC coupling workflow were in good agreement with electronic structure calculations. It is worth emphasizing that our parallel MD-MC coupling scheme using the novel *virtual* atoms is generic in design and requires no apriori information about the defect and chemical environment of the system in question; thus, faithfully realizing segregated solute distributions in scenarios ranging from isolated single dislocation to the complex defect environment.

Most importantly, our MC sampling had no inherent bias with no apriori information on defect geometry and current solute distribution. For each trial move, the probability of being chosen for a particle swap was the same for each *virtual* atom ($p_V = 1/N_V$) and *real* carbon atom ($p_C = 1/N_C$)). In other words, the probability of choosing an arbitrary *virtual* atom and a *real* atom was equally likely. Such a combination of MD-MC coupling with *virtual* atoms and an unbiased sampling approach gave our approach the unique feature of modeling solute segregation in the crystalline *host* system with arbitrary defects. Also, we extensively investigated the aspects of biased sampling [43] and localized trial moves [47] in our previous works. Furthermore, parallelization of MD-MC coupling [42,43,46,47] was proven to be crucial considering scalability so that larger systems with some microstructure complexity shall be realized. Herein, for our MD-MC simulations, we assumed a fixed global concentration of solute C atoms, in line with our aim to model solute segregation in an alloy model with predefined stoichiometry and arbitrary defects (e.g., as a result of processing). In principle, one could also realize a system with an external reservoir of solute C atoms in an unperturbed system (e.g., like the lower region of the model as shown in Fig. 7 Top row), such that the total number of carbon atoms (N_C) could fluctuate.

Effects of initial C concentration: We extended our parallel MD-MC coupling framework to validate its robustness for atomic configurations with different initial background C concentrations. Fig. 7 (top row) shows the homogenous distribution of four different C (*red*) concentrations (i.e., 0.0025, 0.005, 0.010, and 0.020 wt.%). The pixelated regions indicate moderate to high geometrically necessary dislocations (GND) values, correlating with existing dislocations caused by nanoindentation. Across all the configurations simulated with MD-MC coupling, after 0.35×10^6 MC steps, we observed a qualitative trend of C atoms segregating toward regions with considerable GND values (refer Fig. 7 (bottom row)).

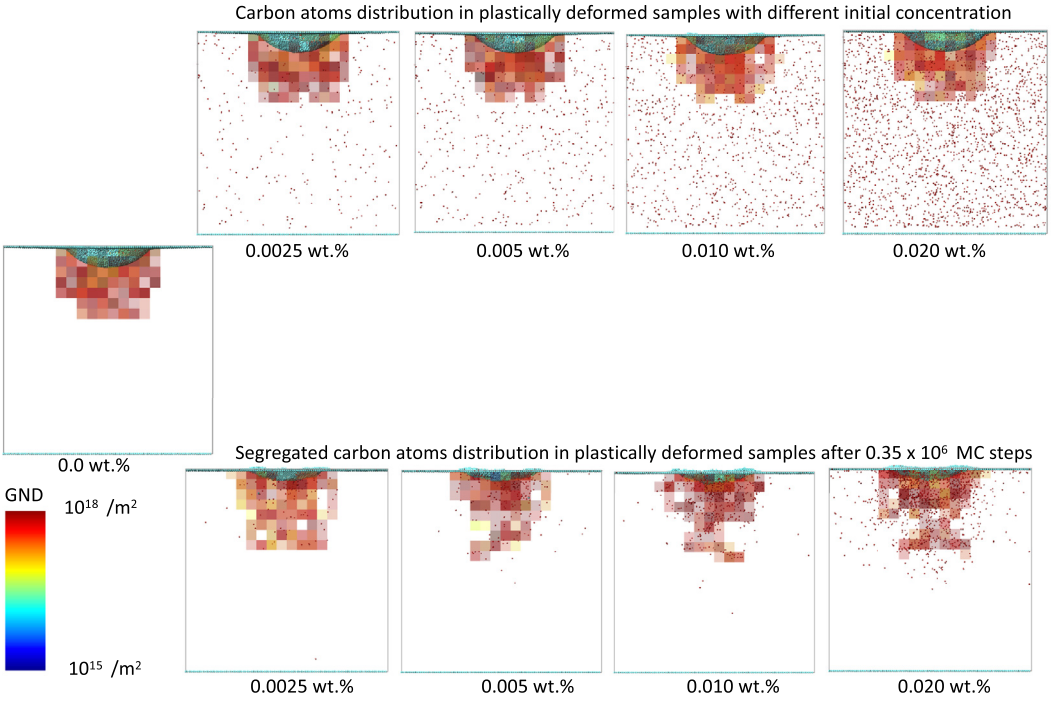

Fig. 7. Top row: Nanoindented samples from Global MD with different initial background C concentrations, i.e., 0.0025, 0.005, 0.010 and 0.020 wt.% The pixelated color code indicates GND. Only C atoms (*red*) are shown for visual clarity. Bottom row: Atomic configurations showing segregated C atoms after 0.35×10^6 MC steps.

However, for the high C concentration model with 0.020 wt.% C, we observed a smearing pattern of C atoms at spatial regions outside GND pixels in the upper half of the simulation domain (refer Fig. 7 bottom row (last)).

The reasons behind such a smearing pattern (for a high C concentration, i.e., 0.020 wt.%) could be twofold: 1) a series of segregated C atoms in a spatially confined region near defects could reach the local C concentration limit and, therefore, not energetically favorable due to C-C repulsion. We justify this argument by observing a similar C-smearing pattern in other Fe-C systems from our previous studies [42,44] with single dislocations. 2) Also, sampling probability is considerably lowered with increasing C atoms while comparing all four configurations after 0.35×10^6 MC steps. Another interesting aspect is to observe some slight changes in the GND distribution profile after 0.35×10^6 MC steps, resulting from a series of localized energy minimization; thus, the effects of solute-defect interaction. Furthermore, our results revealed no or few carbon atoms existed in the lower half of the crystal spanning 15 nm, indicating the executed MC steps sufficiently spanned the whole simulation domain, regardless of the initial C concentration.

To the author's best knowledge, no previous works reported such physically informed modeling of solute segregation (Cottrell atmosphere) in crystalline material with arbitrary defects using off-lattice atomistic simulations, combining efficient parallelization and scalability.

Investigating local C solubility limit: To unravel the origin of the local C solubility limit and its spatial correlation with defect sites, we computed local C concentration in the final configuration yielded by MD-MC coupling. Recall that a final configuration contained segregated C distribution and crystalline defects like dislocations networks.

In the final configuration, local atomic C concentration was computed by constructing a sphere of radius, $r_{\text{conc}} = 1$ nm around each C atom. Fig. 8 shows such computed local C concentration field map on the perspective projected computational domain. To obtain spatially relevant information, the configurations were sliced at the selected coordinates interval (refer to slice markers (a–i) in Fig. 8), and each sliced portion spans the thickness, $t = 4$ Å. Herein, sliced slabs along the X (a (146–150 Å), b (176–180 Å), c (256–260 Å)), Y (d (56–60 Å), e (156–160 Å), f (256–260 Å)), and Z (g (136–140 Å), h (276–280 Å), and i (286–290 Å)) directions at selected intervals aid in visualizing C distribution and quantifying their respective local concentrations in the nanoindented sample. In Fig. 8, the slices along the X ('a'and 'b') and Y (refer 'e') showed high local C concentration (1.5–2.0 at.%.) in the vicinity of the surface crater created by the spherical indenter. Also, considerable concentration (0.25–1.75 at.%.) was observed near the dislocation core region. Whereas the sliced configurations (refer to 'c', 'f' in Fig. 8) exhibited low C concentration along the surface, as it was near the periphery of the crater region. Negligible or nearly zero local C concentrations were observed in the lower half of the computational domain along the Z direction, as there were no significant traces of distortion, validating our previous results and discussion on C segregation profiles. Therefore, sliced configurations (refer to 'h' and 'i' in Fig. 8) were intentionally made in the upper half of the simulation domain.

To this end, our investigation revealed the distribution of local C concentration by probing the entire computational domain, however, by making slices at selective locations both near the surface crater and lattice distortion regions (i.e., moderate-high GND). We propose two possible reasons for such C distribution: 1) hierarchical solute-defect interaction energy and 2) interaction between different dislocations and strain fields:

Hierarchical solute-defect interaction energy: While performing MC trial moves, some C atoms sampled near the crater region were energetically favorable relative to dislocation or defect regions. Consequently, our results emphasize that both the crystalline defect dimensionality, e.g., vacancies (0D), dislocations (1D), grain boundaries (2D), and their associated strain fields govern the energetics of the solute-defect interaction and the resulting segregation profile. In other words, C atoms tended to segregate at or near defect regions that were more energetically favorable.

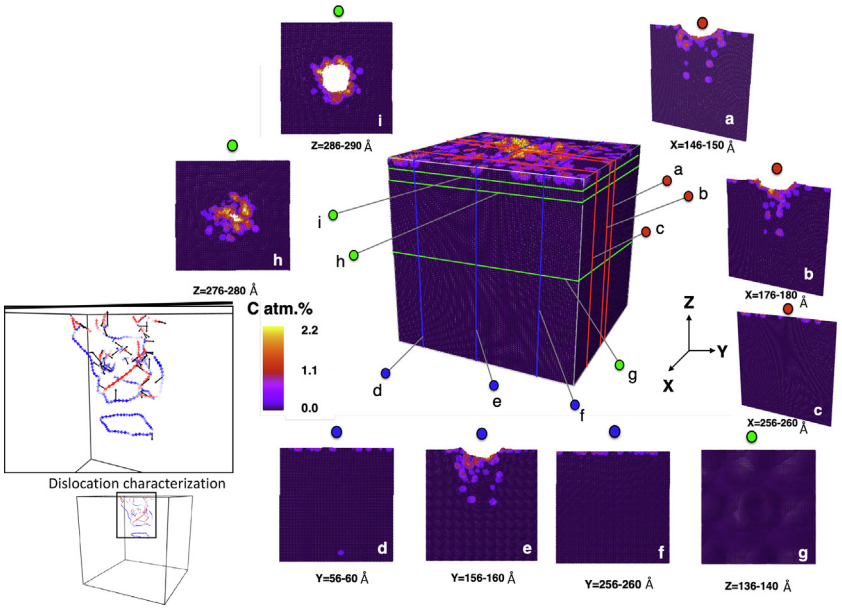

Fig. 8. The final configuration from MD-MC coupling color-coded after local atomic C concentration. Markers (a–i) indicate sliced regions along with their coordinates range for unraveling spatial correlation of local C concentration and defect regions (e.g., GND). Inset represents the dislocation characterization as follows: edge (blue), screw (red) and mixed (gradient).

Interaction between dislocations and strain fields:

Interactions between dislocations and their types determine the resulting strain field in the atomic neighborhood. For instance, when an attractive force field exists between two dislocations, they get drawn to each other and annihilated. In such a scenario, local strains were utilized to rearrange the atomic planes and make them less energetically favorable [42]. The dislocations in the nanoindented sample were extracted using the visualization package OVITO [49] to gain more insights regarding the aforementioned possibilities. Extracted dislocations and their types are shown in the Fig. 8 inset. Altogether, 52 dislocation segments were detected, spanning 145.9 Å and with three major dislocation types: $1/2 < 1\ 1\ 1 >$, $< 1\ 0\ 0 >$, and $<1\ 1\ 0>$. For visualization, we color-coded the dislocation segments as follows: edge dislocations (blue), screw dislocations (red), and color gradient for mixed dislocations. Furthermore, dislocations were characterized by the line vector (as body arrows) and the Burgers vector (as black arrows). To this end, we observed many C atoms segregated towards the crater region, followed by the edge dislocation (lined up along the core) segments in the network. The screw dislocations exhibited triple junctions, thus, eventually providing less energetically favorable sites for C atoms segregation. Thus, a diffusing C atom experiences the least resistance and more room from the atomic neighborhood in regions with a tensile strain. On the other hand, a compressive strain field provides less room for the interstitial C solutes, resulting in low segregation in those regions. Consequently, regions with tensile strains were more preferred energetically for solute segregation [15,16,19,22].

4. Conclusions

Metallic materials, especially alloys, encompass crystalline defects due to processing and heat treatments. Due to low solubility, solutes segregate towards these defects, resulting in an inhomogeneous cloud-like distribution called the Cottrell atmosphere. Such microscopic interactions between segregated solute clouds and defects contribute to macroscopically observed strengthening phenomenon (i.e., higher yield strength). Obtaining physically informed solute-segregated patterns in alloys remains a challenge in unraveling the complex segregated solutes-defect interaction. This work addressed this challenge by realizing an MD-MC atomistic framework using a novel concept called *virtual* atoms, which are non-physical per definition, exhibiting uni-directional chemical interaction with the host *real* (Fe and C) system. These *virtual* atoms assumed a dual role by displacing to new positions accounting for local lattice distortion (in the scope of MD) and acting as potential sampling sites (in the scope of MC). To this end, we applied this framework to model C solute segregation in the α-Fe (bcc) system. Our MD simulations provided both qualitative and quantitative validations that the *virtual* atoms are not chemically influencing the atomic trajectories of the *real* Fe-C system. One of the salient features of *virtual* atoms is that they sense any dynamic lattice distortion in the system (e.g., defect nucleation) and rearrange to new energetically favorable sites with no apriori information about the solute concentration and defect geometry.

Then, we simulated nanoindentation to plastically deform the atomistic model (i.e., Fe-C) with no apriori expectations on the resulting defect configuration. Note that the phenomena of plastic deformation (*defect nucleation*) and carbon segregation evolve at different time scales separated by orders of magnitude. Herein, the objective is to realize the *nearly* final atomic configuration containing segregated carbon atoms but not simulate the kinetics of carbon diffusion events. Thus, the atomic configuration containing arbitrary defects and homogeneously distributed C atoms (simulated with *Global* MD) will be given as the input configuration for modeling solute segregation (MD-MC coupling). Our coupling framework yielded the final configuration after 1×10^6 MC steps, showing rich inhomogeneous C distributions near dislocations and surface craters. Furthermore, starting with different initial global C concentrations, our simulations yielded consistently segregated C solutes, such that all C atoms migrated from less crystalline distortion to high crystalline distortion regions. Due to the local C solubility limit, segregated C atoms smear out near the defect at the high C concentration. Besides unraveling the strong spatial correlation between local C concentration and defect regions, they also revealed two crucial aspects of preference: 1) defect energetics hierarchy and 2) tensile strain field near the dislocations.

To the author's best knowledge, we first reported modeling off-lattice solute segregation in such plastically deformed samples with arbitrary defect and chemical complexity. To this end, our results demonstrate the capability of obtaining physically informed solute-segregated configurations with no apriori information on favorable sites and defect geometry. These unique features of our MD-MC coupling framework were possible through *virtual* atoms. Although we proved the application of our proposed coupling framework for realizing solute segregation in a deformed single crystal with dislocation networks, the core concept remains amenable to other complex scenarios like poly-nanocrystalline systems. Our MD-MC coupling approach with the *virtual* atoms enables unraveling complex segregated solutes-defect interaction in alloys at atomic resolution.

Data availability

The raw/processed data required to reproduce these findings cannot be shared at this time as the data also forms part of an ongoing study.

Declaration of competing interest

The authors declare that they have no known competing financial interests or personal relationships that could have appeared to influence the work reported in this work.

CRediT authorship contribution statement

Hariprasath Ganesan: Conceptualization, Methodology, Software, Visualization, Validation, Formal analysis, Writing – review & editing. **Godehard Sutmann:** Conceptualization, Resources, Supervision, Writing – review & editing.

Acknowledgments

The authors gratefully acknowledge the funding from the German Research Foundation (DFG) - BE 5360/1-1 and ThyssenKrupp Europe. They acknowledge the computing time granted through JARA-HPC on the supercomputer JURECA at Forschungszentrum Jülich. The authors greatly acknowledge the funding acquisition, scientific discussions, and support for project supervision from Christoph Begau and Alexander Hartmaier. Hariprasath Ganesan thanks Stefan Sandfeld for some fruitful discussion, mentoring, and encouragement.

References

[1] A. Cottrell, B. Bilby, Proc. Phys. Soc. Sect. A 62 (1949) 49.
[2] D. Blavette, E. Cadel, A. Fraczkiewicz, A. Menand, Science 286 (1999) 2317–2319.
[3] J. Wilde, A. Cerezo, G. Smith, Scr. Mater. 43 (2000) 39–48.
[4] F. Nabarro, Mater. Sci. Eng. A 400 (2005) 22–24.
[5] M. Miller, Microsc. Res. Tech. 69 (2006) 359–365.
[6] J. Takahashi, K. Kawakami, J. Hamada, K. Kimura, Acta Mater. 107 (2016) 415–422.
[7] V. Yamakov, D. Wolf, S. Phillpot, A. Mukherjee, H. Gleiter, Nat. Mater. 3 (1) (2004) 43–47.
[8] L. Malerba, D. Terentyev, P. Olsson, R. Chakarova, J. Wallenius, J. Nucl. Mater. 329 (2004) 1156–1160.
[9] Y. Li, A. Goyal, A. Chernatynskiy, J. Jayashankar, M. Kautzky, S. Sinnott, S. Phillpot, Mater. Sci. Eng. A 651 (2016) 346–357.
[10] H. Ganesan, I. Scheider, C. Cyron, Front. Mater. 7 (2021) 602567.
[11] H. Ganesan, I. Scheider, C. Cyron, Mater. Des. 212 (2021) 110282.
[12] C. Liu, X. Zhu, X. Li, Q. Shi, Powder Technol. 398 (2022) 117069.
[13] A. Chandran, H. Ganesan, C. Cyron, Mater. Des. 237 (2024) 112596.
[14] Y. Wang, D. Srolovitz, J. Rickman, R. Lesar, Acta Mater. 48 (2000) 2163–2175.
[15] B. Soenen, A. De, S. Vandeputte, B. De Cooman, Acta Mater. 52 (2004) 3483–3492.
[16] Q. Chen, X.-Y. Liu, S. Biner, Acta Mater. 56 (2008) 2937–2947.
[17] S. Jang, Y. Purohit, D. Irving, C. Padgett, D. Brenner, R. Scattergood, Acta Mater. 56 (2008) 4750–4761.
[18] Y. Hanlumyuang, P.A. Gordon, T. Neeraj, D. Chrzan, Acta Mater. 58 (2010) 5481–5490.
[19] R. Veiga, H. Goldenstein, M. Perez, C. Becquart, Scr. Mater. 108 (2015) 19–22.
[20] L. Zepeda-Ruiz, A. Stukowski, T. Oppelstrup, V. Bulatov, Nature 550 (2017) 492–495.
[21] V. Borovikov, M.I. Mendelev, A. King, Int. J. Plast. 90 (2017) 146–155.
[22] M. Pascuet, G. Monnet, G. Bonny, E. Martínez, J. Lim, M. Burke, L. Malerba, J. Nucl. Mater. 519 (2019) 265–273.
[23] B. Zhang, Y. Guo, Z. Liu, M. Li, D. Shi, Y. Li, J. Song, M. Bu, S. Du, J. Alloy. Compod. 857 (2021) 157486.
[24] B. Sadigh, P. Erhart, A. Stukowski, A. Caro, E. Martinez, L. Zepeda-Ruiz, Phys. Rev. B 85 (2012) 184203.
[25] E. Picard, F. Sansoz, Acta Mater. 240 (2022) 118367.
[26] J. Mitchell, F. Abdeljawad, C. Battaile, C. Garcia-Cardona, E. Holm, E. Homer, J. Madison, T. Rodgers, A. Thomson, V. Tikare, E. Webb, S. Plimpton, Model. Simul. Mater. Sci. Eng. 31 (2023) 055001.
[27] R. Veiga, M. Perez, C. Becquart, E. Clouet, C. Domain, Acta Mater. 59 (2011) 6963–6974.
[28] J. Yan, C. Wang, W. Duan, S. Wang, Phys. Rev. B 69 (2004) 214110.
[29] J. Stadler, R. Mikulla, H.-R. Trebin, Int. J. Mod. Phys. C 8 (1997) 1131–1140.
[30] M. Daw, M. Baskes, Phys. Rev. B 29 (1984) 6443.
[31] R. Veiga, C. Becquart, M. Perez, Comput. Mater. Sci. 82 (2014) 118–121.
[32] M. Ruda, D. Farkas, G. Garcia, Comput. Mater. Sci. 45 (2009) 550–560.
[33] C. Becquart, J. Raulot, G. Bencteux, C. Domain, M. Perez, S. Garruchet, H. Nguyen, Comput. Mater. Sci. 40 (2007) 119–129.
[34] S. Plimpton, J. Comput. Phys. 117 (1995) 1–19.
[35] D. Perez, B. Uberuaga, Y. Shim, J. Amar, A. Voter, Annu. Rep. Comput. Chem. 5 (2009) 79–98.
[36] S. Chakraborty, J. Zhang, S. Ghosh, Comput. Mater. Sci. 121 (2016) 23–34.
[37] H. Ganesan, On the potential benefits of using GPUs for atomistic MD simulations using LAMMPS, https://zenodo.org/records/10539114(2022).
[38] Y. Pang, D. Sun, Q. Gu, K.-C. Chou, X. Wang, Q. Li, Crystal Growth Des. 16 (2016) 2404–2415.
[39] Q. Luo, Y. Guo, B. Liu, Y. Feng, J. Zhang, Q. Li, K. Chou, J. Mater. Sci. Technol. 44 (2020) 171–190.
[40] Q. Li, Y. Lu, Q. Luo, X. Yang, Y. Yang, J. Tan, Z. Dong, J. Dang, J. Li, Y. Chen, B. Jiang, S. Sun, F. Pan, J. Magnes. Alloy. 9 (2021) 1922–1941.
[41] Q. Li, X. Lin, Q. Luo, Y. Chen, J. Wang, B. Jiang, F. Pan, Int. J. Miner. Metall. Mater. 29 (2022) 32–48.
[42] H. Ganesan, C. Begau, G. Sutmann, in: Simulation Science: First International Workshop, SimScience 2017, Göttingen, Germany, April 27–28, 2017, Springer, 2018, pp. 112–127.
[43] H. Ganesan, M. Longsworth, G. Sutmann, J. Phys. Conf. Ser. 1740 (2021) 012001.
[44] H. Ganesan, Highly Parallel Molecular Dynamics/Monte Carlo Coupling Towards Solutes Segregation Modelling, Ruhr Univerity Bochum, 2019, Ph.D Thesis.
[45] G. Sutmann, H. Ganesan, C. Begau, in: AIP Conference Proceedings, 1863, 2017.
[46] C. Teijeiro, R. Halver, H. Ganesan, G. Sutmann, W. Homberg, in: The Fifth International Conference on Parallel, Distributed, Grid and Cloud Computing for Engineering, Jülich Supercomputing Center, 2017.
[47] H. Ganesan, C. Teijeiro, G. Sutmann, Comput. Mater. Sci. 155 (2018) 439–449.
[48] C. Begau, A. Hartmaier, E. George, G. Pharr, Acta Mater. 59 (2011) 934–942.
[49] A. Stukowski, Model. Simul. Mater. Sci. Eng. 18 (2009) 015012.